Shape Recovery from Equal Thickness Contours

Ge Cong, *Member*, *IEEE*, and
Bahram Parvin, *Senior Member*, *IEEE*

Abstract—A unique imaging modality based on Equal Thickness Contours (ETC) has introduced a new opportunity for 3D shape reconstruction from multiple views. These ETCs can be generated through an interference between transmitted and diffracted beams. We present a computational framework for representing each view of an object in terms of its *object thickness* and then integrating these representations into a *3D surface* by algebraic reconstruction. In this framework, the object thickness is first derived from ideal contours and then extended to real data. For real data, the object thickness is inferred by grouping curve segments that correspond to points of second derivative maxima. At each step of the process, we use some form of regularization to ensure closeness to the original features as well as neighborhood continuity. We apply our approach to images of a submicron crystal structure obtained through a holographic process.

Index Terms—Shape-from-X, 3D construction, shape from multiple views.

◆

1 INTRODUCTION

THE problem of shape-from-X has been a central research topic in the computer vision community. These include, but are not limited to, shape from shading, texture, contour, color, etc. These techniques have been applied in a number of ways, from images obtained in controlled environments to natural outdoor scenes that may include more than one view. In this paper, we introduce an imaging modality and the corresponding method for shape recovery, which has not yet been addressed by the computer vision community [7], [6]. This modality is based on equal thickness contour (ETC), obtained through either extinction oscillation (at low resolution) or holographic process (at high resolution) [11], [22]. Extinction oscillation encodes changes in the thickness as a periodic pattern (fringes) and holographic microscopy constructs this periodic pattern by interference between a reference and a hologram. This is tangentially related to radar interferometry [1], [12], [17], [18] for change detection. Radar interferometry relates time evolution to phase information, whereas holographic microscopy relates thickness evolution to phase data. In the latter case, the periodicity in the gray level can be mapped to the changes in the thickness. Here, there is no phase unwrapping problem because time and phase are not wrapped around. In this paper, we focus on magnitude information, corresponding to the equal thickness contours, to construct a 3D surface.

Fig. 1 shows a simulation of ETCs for a synthetic object. The main issue is that this mode of representation is inherently ambiguous since objects with completely different geometry can produce similar ETCs. For example, a sphere and a half sphere generate the same set fringe contours. This mode of imaging is different from radar interferometry since fringe contours do not encode height or altitude information. Fig. 2 shows three views of a real crystal structure that will be used for shape recovery. A small angle of rotation between these views is indicated by the changes in the fringe patterns.

A critical step in recovering the shape from multiple views is the representation of each view of an object in terms of its thickness. This representation is derived from ETCs that are difficult to compute from real images. Hence, we first introduce a solution for recovering the thickness map for idealized perfect data and then show how this technique can be extended to real data. In the case of synthetic data, the problem reduces to "shape from sparse fringe contours," where a novel solution based on an *equal importance criterion* is introduced. This constraint weighs each point in the image identically; it is expressed in a functional form and then minimized using variational principles. In the case of real images, we introduce a series of steps to recover the relevant features in the image, as shown in Fig. 3. The dominant features in these images are roof and trough edges corresponding to crease lines; however, it is well-known that it is difficult to extract these features directly in the presence of scale-change and noise. Here, we have adopted a stepwise refinement of images to extract a desirable representation. The first step of the process enhances peaks and valleys of the original data with adaptive smoothing. Next, crease points are extracted and grouped on the basis of collinearity and convexity. It is assumed that grouping does not produce closed contours and an interactive snake is provided to establish the boundary conditions, based on innermost and outermost fringes.[1] The grouping strategy is very conservative to allow closure of small gap and to provide the necessary coupling so that segments from adjacent fringes are not grouped together (e.g., there is no crisscrossing). The contour representation (based on lines of second derivative maxima) provides the basis for obtaining object thickness at each point in the image. We have developed a regularized approach to computing object thickness, subject to continuity and smoothness constraints. The final step of our protocol is to integrate object thicknesses obtained from each viewing orientation into a 3D surface representation. The approach is based on a modification and extension of the algebraic reconstruction technique [14], [15] process.

In the rest of this paper, we first introduce a recovery of thickness map from idealized contour data. In Section 3, we introduce the steps required to recover the thickness map for real data. In Section 4, the details of multiple view integration are outlined, followed by concluding remarks in Section 5.

2 OBJECT THICKNESS FROM IDEAL CONTOURS

The problem of shape from sparse data has been extensively studied in the computer vision and visualization community, as indicated in an excellent review by Bolle and Vemuri [5]. Although fringe contours are considered to be sparse, existing techniques are not applicable because the data is less dense, but well-organized. Another area related to our research problem is surface reconstruction from slice contours, which has been studied in computer graphics and medical image processing. However, these techniques assume that slices are very close to each other, which may not always be true. Furthermore, this technique [4] is based on Delaunay triangulation and thus is scale dependent.

We propose to solve this ill-posed problem by enforcing the *Equal Importance Criterion*, which suggests that all points contribute equally to the shape reconstruction problem. Formally, the constraint states that surface height decreases linearly along the trajectory of its gradient and, as a result, the problem becomes well-posed. Because the solution for the system of partial differential equations (PDE) may not always exist, we redefine it as a variational problem to minimize the change in gradient over the region where the fringe contours are defined.

- *The authors are with Computing Sciences, Lawrence Berkeley National Laboratory, MS 50B-2239, 1 Cyclotron Road, Berkeley, CA 94720.*
E-mail: {gcong, parvin}@media.lbl.gov.

Manuscript received 6 June 1998; accepted 30 Nov. 1999.
Recommended for acceptance by G. Medioni.
For information on obtaining reprints of this article, please send e-mail to: tpami@computer.org, and reference IEEECS Log Number 107689.

[1] The emphasis is on having a robust system so that the science project can proceed uninterrupted.

U.S. Government Work Not Protected by U.S. Copyright

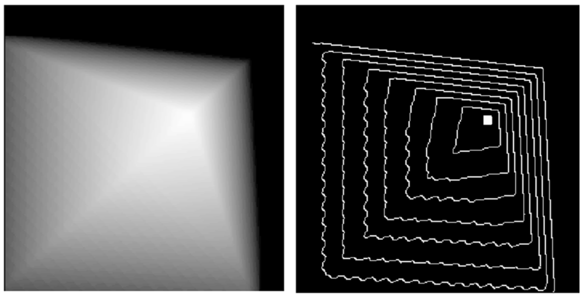

Fig. 1. (a) Thickness of a synthetic pyramid and (b) the corresponding equal thickness contours.

2.1 Fringe Representation

Fringes may be defined mathematically in the following way: Let the 3D surface $f(x,y)$ be in a simply connected region $(x,y) \in D$ with continuous first order derivatives. Fringe contours $(\mathcal{C}_i)$ can be defined as:

$$\mathcal{C}_i = \{(x,y) | f(x,y) = i \cdot \triangle\xi\}, \qquad i = 1, ..., m, \tag{1}$$

where $\triangle\xi$ is a constant and relates to the wave-length of the interferometry system. Without loss of generalities, we assume that $\triangle\xi = 1$. $f(x,y)$ is further constrained so that $\mathcal{C}_i$ has the following properties:

1. $\mathcal{C}_i$ is totally enclosed by $\mathcal{C}_j$ if and only if $i > j$.
2. The width of $\mathcal{C}_i$ is 0 (1 in the discrete case), i.e., the surface does not have flat regions.

Let $R(\mathcal{C}_1, \mathcal{C}_m)$ be the doubly or multiply connected region enclosed by $\mathcal{C}_1$ and $\mathcal{C}_m$, as shown in Fig. 4. The inverse problem can now be expressed as:

$$\begin{aligned} &Given\ \mathcal{C}_i, i = 1, ..., m, find\ f(x,y), \\ &\qquad where\ (x,y) \in R(\mathcal{C}_1, \mathcal{C}_m), such\ that\ f(\mathcal{C}_i) = i. \end{aligned}$$

2.2 Equal Importance Criterion

First, consider a simplified example in which we have only two contours $\mathcal{C}_1$ and $\mathcal{C}_2$. In $R(\mathcal{C}_1, \mathcal{C}_2)$, we want to construct a surface $f(x,y)$ such that $f(\mathcal{C}_1) = 1, f(\mathcal{C}_2) = 2$. Obviously, in the absence of any constraints, infinitely many solutions exist. To constrain the problem, we assert that *every point between* $\mathcal{C}_1$ and $\mathcal{C}_2$ *is equally important and contributes similarly to the reconstruction process. Any other assumption means that we know something about the surface.* We call this the *Equal Importance Criterion*.

This constraint is formalized by requiring that the change in the gradient-magnitude along the gradient direction should be zero, that is:

$$\mathcal{J}_1(f) = \bigtriangledown(|\bigtriangledown f|) \cdot \frac{\bigtriangledown f}{|\bigtriangledown f|} = 0, \tag{2}$$

where $\bigtriangledown f$ indicates the gradient of f, $|\ |$ the norm, and $\cdot$ the inner product. The above PDE implies that, along each trajectory of the gradient of the surface, the magnitude of the gradient is a constant. In another words, the height decreases linearly from, say, 2 to 1. The level curves of f, which can be considered as the interpolation of $\mathcal{C}_1, \mathcal{C}_2$, are equally distributed along the gradient. Thus, in a view of height, which is our only clue about the surface, all points are equally important.

$\mathcal{J}_1$ can be rewritten as:

$$\begin{aligned} \mathcal{J}_1 &= \frac{\partial}{\partial x}\left(\sqrt{f_x^2 + f_y^2}\right)\frac{f_x}{\sqrt{f_x^2 + f_y^2}} + \frac{\partial}{\partial y}\left(\sqrt{f_x^2 + f_y^2}\right)\frac{f_y}{\sqrt{f_x^2 + f_y^2}} \\ &= \frac{f_x^2 f_{xx} + 2 f_x f_y f_{xy} + f_y^2 f_{yy}}{f_x^2 + f_y^2}. \end{aligned} \tag{3}$$

Thus, (2) can be reduced to:

$$\mathcal{J}_2(f) = f_x^2 f_{xx} + 2 f_x f_y f_{xy} + f_y^2 f_{yy} = 0, \tag{4}$$

where subscript indicates derivative, such as $f_x = \frac{\partial f}{\partial x}, f_{xy} = \frac{\partial^2 f}{\partial x \partial y}$. Thus, the problem becomes:

$$\begin{aligned} &Find\ \ f(x,y), \quad (x,y) \in R(\mathcal{C}_1, \mathcal{C}_2), \\ &such\ that\ \ \mathcal{J}_2(f) = 0, \quad f(\mathcal{C}_1) = 1, \quad f(\mathcal{C}_2) = 2. \end{aligned} \tag{5}$$

Equation (4) is called the "Infinity Laplacian" (see the Appendix), which has been studied in detail [2], [3], [8]. Equation (5) has several important properties:

1. There is at most one solution of Dirichlet's problem for f. There is not always a smooth solution for any $\mathcal{C}_1$ and $\mathcal{C}_2$. However, if we redefine the "solution" in a suitably weak sense, the solution does exist.
2. The trajectory of the vector field for $\bigtriangledown f$ is either a convex curve or a straight line.
3. A solution is infinitely differentiable if the trajectories of $\bigtriangledown f$ are convex curves.

All these properties are correct only in $R(\mathcal{C}_1, \mathcal{C}_2)$, where the value of f is known only on the boundaries.

2.3 Reconstruction of Object Thickness

It is natural to extend (5) to $R(\mathcal{C}_1, \mathcal{C}_m)$:

$$\begin{aligned} &Find\ \ f(x,y), \quad (x,y) \in R(\mathcal{C}_1, \mathcal{C}_m), \\ &such\ that\ \ \mathcal{J}_2(f) = 0, \quad f(\mathcal{C}_i) = i, \quad i = 1, ..., m. \end{aligned} \tag{6}$$

However, this is an overconstrained problem, which may not always have an *exact* solution. To show that there may not be a solution, suppose that we have two sets of contours $\mathcal{C}_1, \ldots, \mathcal{C}_{i-1}, \mathcal{C}_{i+1}, \ldots, \mathcal{C}_m$ and $\mathcal{C}_1, \ldots, \mathcal{C}_{i-1}, \mathcal{C}_i', \mathcal{C}_{i+1}, \ldots, \mathcal{C}_m$ such that $\mathcal{C}_i' \neq \mathcal{C}_i$. Their solutions should then be different. On the other

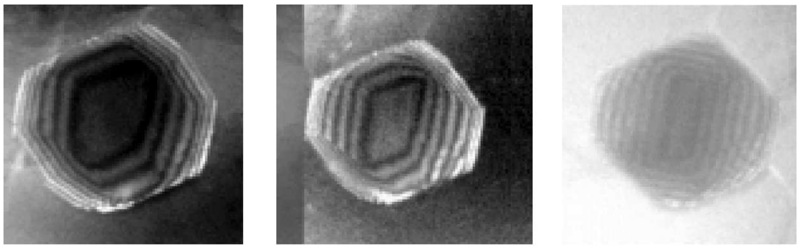

Fig. 2. Three views of a cubeoctahedral object with a diameter of 100 nanometer.

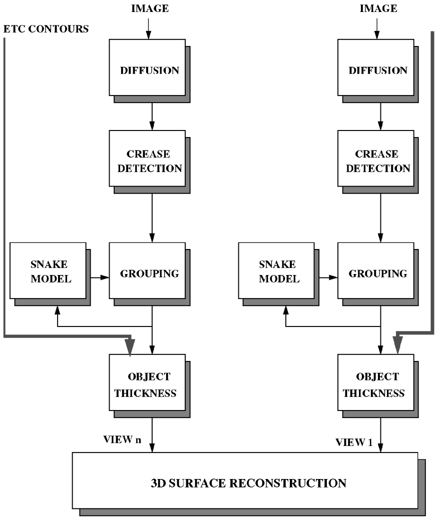

Fig. 3. Protocol for recovering 3D shape from interference patterns.

hand, since they have the same $R(\mathcal{C}_1, \mathcal{C}_m)$ and f has a unique solution for $\mathcal{J}_2 = 0$ in $R(\mathcal{C}_1, \mathcal{C}_m)$, the two set of contours must have the same solutions. The conflict means that at least one set of contours does not have a solution. We thus seek a solution to the following problem:

$$\begin{aligned} &Minimize \quad \varepsilon^2 = \int\int_{R(\mathcal{C}_1,\mathcal{C}_m)} \mathcal{J}_1^2 dxdy,\\ &Subject\ to: \quad f(\mathcal{C}_i) = i, \quad i = 1, ...m. \end{aligned} \tag{7}$$

We use $\mathcal{J}_1$ instead of $\mathcal{J}_2$ in (7) because, on the surface we will generate, $\mathcal{J}_1$ is not always equal to 0. Thus, it cannot be reduced to $\mathcal{J}_2$. In another words, $\mathcal{J}_2$ cannot describe the EIC in this situation. f can be solved iteratively by $f^{v+1} = f^v - \sigma\delta f^v$, where σ is the step size, v indicates the iteration number, and δf is the variation of f:

$$\delta f = -\frac{\partial \mathcal{F}_{f_x}}{\partial x} - \frac{\partial \mathcal{F}_{f_y}}{\partial y} + \frac{\partial^2 \mathcal{F}_{f_{xx}}}{\partial x^2} + \frac{\partial^2 \mathcal{F}_{f_{xy}}}{\partial x \partial y} + \frac{\partial^2 \mathcal{F}_{f_{yy}}}{\partial y^2}. \tag{8}$$

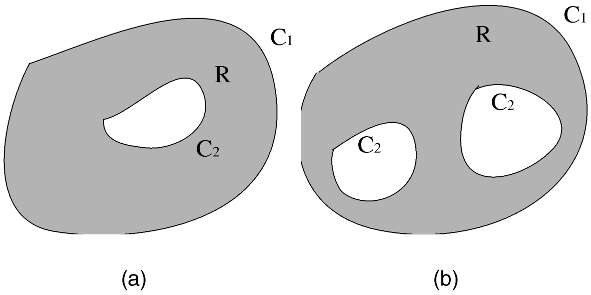

Fig. 4. $R(\mathcal{C}_1, \mathcal{C}_m)$: (a) Doubly connected region. (b) Multiply connected region.

2.4 Initialization

A good initialization is very important for deriving the solution to the desired local minima. This is accomplished by distance transformation. Let $d_i(x, y)$ be the *Distance Transformation* of curve C_i, where it is negative inside C_i and positive outside C_i. First, we represent $d_i(x, y)$ $i = 1, \ldots, m$ as the Chamfer image of the fringes. Then, $f(x, y)$, $(x, y) \in R(\mathcal{C}_i, \mathcal{C}_{i+1})$ is approximated as follows:

$$f(x, y) = \frac{d_i(x, y) \cdot (i + 1) - d_{i+1}(x, y) \cdot i}{d_i(x, y) - d_{i+1}(x, y)}. \tag{9}$$

This step specifies the boundary condition for innermost and outermost contours at $f(\mathcal{C}_i) = i$. These boundary conditions are not updated during the regularization process.

2.5 Experimental Results from Ideal Contours

We have tested our method on both synthetic and real fringe contours. Fig. 5 shows the computed surface of the synthetic contours with various degrees of complexity. Fig. 6 and Fig. 7 show the surface reconstructed from real data, interference image. The ETCs were interactively retrieved from the corresponding images. In all these images, $\sigma = 0.1$, and the algorithm converges in less than 100 iterations.

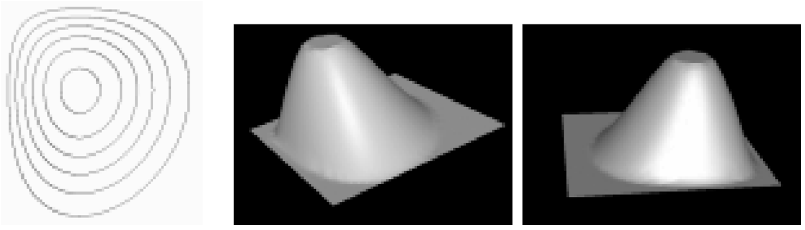

Fig. 5. Reconstruction result: (a) Original fringe contours. (b) and (c) Two views of reconstruction.

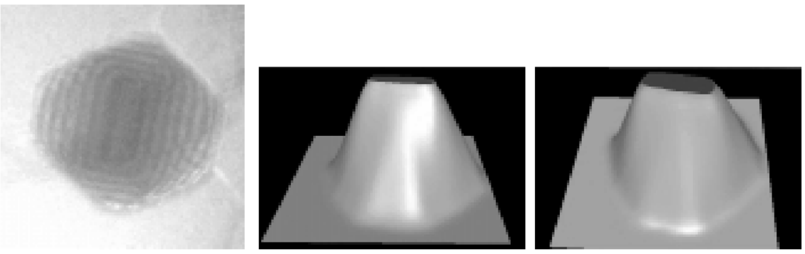

Fig. 6. Reconstruction results of real holographic microscopy image: (a) Images used to generate perfect fringes interactively. (b) and (c) Two views of the corresponding reconstruction result.

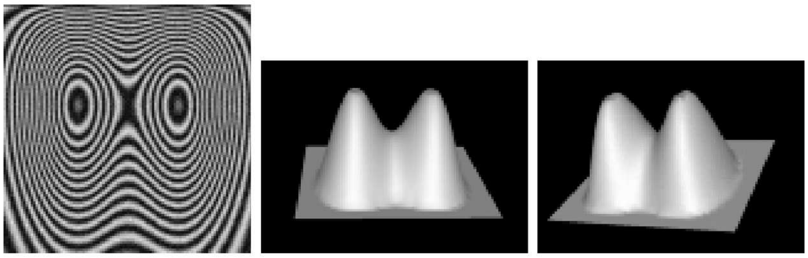
(a) (b) (c)

Fig. 7. Reconstruction results of real optical interference image: (a) Images used to generate perfect fringes interactively. (b) and (c) Two views of the corresponding reconstruction result.

3 OBJECT THICKNESS FROM REAL DATA

Several aspects of surface reconstruction from interferometry patterns have been extensively studied in the remote sensing literature. Radio interferometry provides the phase information, what is known only as modulo 2π, and phase unwrapping techniques either utilize information at every pixel and apply a Fourier transform or use the least square methods to reconstruct the surface [9], [10], [13], [16], [21]. Again, we iterate that the phase unwrapping problem is absent in our case and that interference patterns of our experiment do not necessarily correspond to the height information. Furthermore, this is not the same as the shape from the shading problem because the surface normals are inadequate for inferring the thickness map. In the rest of this section, each step of the process is summarized with the corresponding intermediate results.

3.1 Preprocessing and Grouping

The original images are processed with a variation of adaptive smoothing [20] to enhance the roof edges corresponding to points of local maximum principal curvature where each point in the image is made smoother as a function of its inverse local Laplacian. As a result, when the Laplacian is large, no smoothing is performed. Creases are then localized with the second directional derivative operator. These singular events are linked to form curve segments where sets of curve segments are grouped based on proxmimity, continuity, and convexity. For a detailed description of the crease detection and grouping, see our earlier papers [6], [7].

3.2 Reconstruction of Object Thickness

The goal of reconstructing object thickness is to calculate a 2D image in which each point corresponds to the object thickness in a certain direction. The simple interpolation of Section 2.4 is used to build the initial surfaces between the inner and outer fringes. Next, in the absence of closed contours, local contour segments provide the means for partial correction and updating in a local surface neighborhood. Adjacent contour segments are either parallel or intersect at a small angle. Consider trough T and ridge R contour segments that are adjacent to one another and assume that from T to R the object thickness decreases by a constant, say 1, on the surface. If T and R are parallel with d distance apart (see Fig. 8a) and the thickness decreases linearly, then the magnitude of gradient for points between T and R is given by: $|| \bigtriangledown f|| = \frac{1}{d}$. On the other hand, if the two segments are not parallel (see Fig. 8b), then, for each point p, there should be a curve passing through p that intersects T and R at p_1 and p_2, respectively. The tangent of this curve is in the direction of thickness gradient, which could also be obtained by tracking the gradient direction from p_1 to p_2. Since R and T are level set segments, it is easy to show that the normal to these segments and the gradient of object thickness at any point are in the same direction. When R and T are close to each other and the intersection angle between them is small, we can approximate a curve l, passing through p, by two line segments $pp_1' \perp T, pp_2' \perp R$, where $p_1'pp_2'$ is an approximation of p_1pp_2. Hence, $l \approx |p_1'p| + |p_2'p|$. These line segments are estimated from distance transformations (chamfer images), $d_t(x,y)$ and $d_r(x,y)$, that are computed from trough and ridge segments. Thus, $d_t = |p_1'p|$ and $d_r = |p_2'p|$, and the magnitude of the gradient is given by:

$$|| \bigtriangledown f(x,y)|| = \frac{1}{d_r(x,y) + d_t(x,y)}. \tag{10}$$

3.3 Regularized Object Thickness Construction

The method for object thickness recovery (of Section 2.3) is modified to accommodate the additional gradient thickness information of that earlier section. The motivation is twofold:

1. $\mathcal{C}_i = i$ is no longer available; as a result, the actual thickness is unknown.
2. The computed thickness gradient is noisy and scale limited; as a result, some form of regularization is needed.

We have developed a regularized approach for constructing the object thickness $f(x,y)$. We define a suitable energy function to reflect the closeness to data and a smoothing term:

$$\epsilon^2 = \int\int (f_x - p)^2 + (f_y - q)^2 + \lambda \mathcal{J}_1^2 dxdy, \tag{11}$$

where f_x, f_y denote the x and y derivative of f and p, q are the x and y direction gradient information computed earlier. Note that we do not apply additional constraints to show that the thickness along each segment is constant. However, the first term, $(f_x - p)^2 + (f_y - q)^2$, ensures that the gradient of each point on a segment is perpendicular to the segment. Thus, f is constant along the segment.

Following the Euler Equation, the surface f that minimizes (11) is:

$$(f_{xx} - p_x) + (f_{yy} - q_y) \; - \; \lambda \delta f = 0, \tag{12}$$

where δf is the variation of $\mathcal{J}_1^2$ as defined in the previous section. This equation is solved iteratively from an initial guess

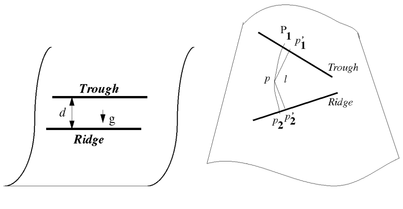

(a) (b)

Fig. 8. Measure of gradient estimates from local contour segments: (a) T and R are parallel. (b) T and R are not parallel.

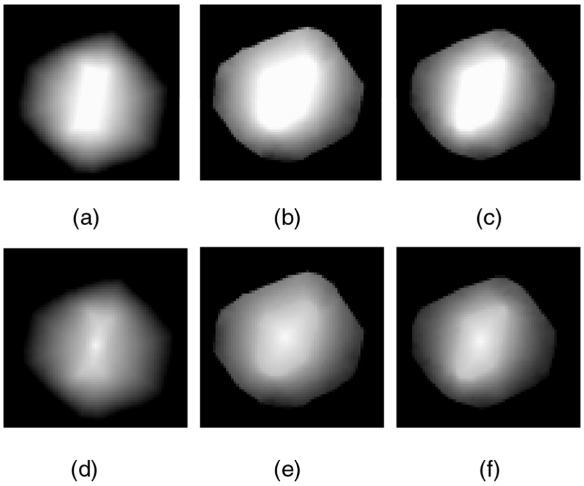

Fig. 9. Reconstructed thickness from the ETC in Fig. 2. (a), (b), and (c) Planar fit. (d), (e), and (f) Interpolating inside inner contour.

corresponding to the interpolation derived from the boundary conditions as indicated by (9).

There is a certain ambiguity in filling up the region inside the inner contour as given by the initial condition. This ambiguity originates from the choice of planar fit or further interpolation from the inner contour to the center of the mass. This is a higher-level process and can only be resolved at the multiple-view integration. Fig. 9 shows the reconstructed object thickness for each view of the object shown in Fig. 2.

4 THREE-DIMENSIONAL SHAPE RECOVERY

In the preceding two sections, we developed an approach to recover the object thickness at each point along a certain direction. This is the thickness between front and back surfaces. In this section, we show how to integrate object thickness representation from different views into a 3D object. The novelty of our work is to reconstruct a binary object from a limited (sparse) number of projections. We only update the boundary of the object and use the simplified curvature of the boundary as the regularization term. This ensures that a smooth object is constructed that is more efficient and converges quickly. Our method extends the algebraic reconstruction techniques (ART) [15], [19] for a small number of views (three in our case) with small angular difference between them (7-8 degrees). The first step is to align the object thickness representation bases in their location at the center of the mass. The 3D object boundary is then initialized as a polytope, which corresponds to the intersection of thickness extremes in 3D space. The 3D surface is then iteratively refined, based on object thickness information from each view. For simplicity, we present the details of our solution in 2D. Let

- $g(i,j)$ be the 2D object image. $g(i,j), i = 0,\dots,I, j = 0,\dots,J$, is a discrete image that represents a binary object A and the background $\bar{A}$:

$$g(i,j) = \begin{cases} 1, & \text{if } (i,j) \in A \\ 0, & \text{if } (i,j) \in \bar{A}. \end{cases} \tag{13}$$

- $\mathcal{P}(\theta,k)$ be the computed thickness from angle θ at a point k, as discussed in previous section,
- $p(\theta,k), -\frac{\pi}{4} \le \theta \le \frac{\pi}{4}$ be the thickness computed from $g(i,j)$. This thickness (as shown in Fig. 10) is given by:

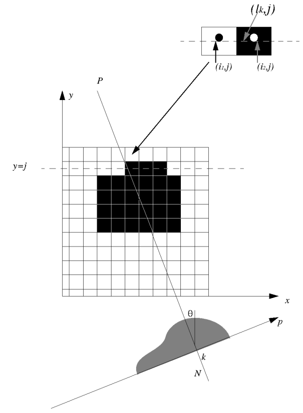

Fig. 10. Projection of a 2D binary image on a line.

$$p(\theta,k) = \sum_{j=0}^{J} \frac{g(l_k,j)}{cos(\theta)}, \tag{14}$$

where (l_k,j) is the intersection point of line PN and the horizontal line $y = j$, and $g(l_k,j)$ is just a linear interpolation of the point around (l_k,j):

$$g(l_k,j) = g(i_1,j) * (i_2 - l_k) + g(i_2,j) * (l_k - i_1). \tag{15}$$

Thus, $p(\theta,k)$ is a linear combination of image pixels $g(i,j), i = 0,\dots,I, j = 0,\dots,J$.

- $b(A), b(\bar{A})$ be the boundary points. The boundary point of the object is defined as:

$$\begin{aligned} b(A) := \{(i,j) | g(i,j) \cap [\bar{g}(i-1,j) \cup \bar{g}(i,j-1) \\ \cup\, \bar{g}(i+1,j) \cup \bar{g}(i,j+1)] = 1\}, \end{aligned} \tag{16}$$

where $\cap$ and $\cup$ correspond to the logical *and* and *or* operations. $\bar{g}(i,j)$ is the inverse of $g(i,j)$. Similarly, the boundary point of the background is defined as:

$$\begin{aligned} b(\bar{A}) := \{(i,j) | \bar{g}(i,j) \cap [g(i-1,j) \cup g(i,j-1) \\ \cup\, g(i+1,j) \cup g(i,j+1)] = 1\}. \end{aligned} \tag{17}$$

- $\hat{p} \in b(\bar{A})$ of point $p \in b(A)$ be the neighborhood points, where $\hat{p}$ is defined over a 3-by-3 neighborhood of p in the background and is in the normal direction of the object's occluding contour at point p.

Assume that we have N thicknesses of a 2D object A along N directions $\mathcal{P}(\theta_n,k), n = 0,\dots,N$ and that each thickness has M_n points. To reconstruct an $I \times J$ image $g(i,j)$ for the corresponding thicknesses, we define a cost function:

$$\epsilon^2 = \sum_{n=0}^{N} \sum_{m=0}^{M_n} (p(\theta_n,m) - \mathcal{P}(\theta_n,m))^2 + \lambda \sum_{(i,j)\in b(A)} (\mathcal{K}(i,j))^2, \tag{18}$$

where $\mathcal{K}$ is the product of the curvature of the boundary conditions and $|\bigtriangledown g|^3$ since using the curvature would have complicated the optimization process. We request the curvature along the boundary to be small, which prefers smooth objects. The $\mathcal{K}$ term of the boundary point serves as a penalty term for smoothness and $\mathcal{K}$ is computed from the binary images as:

$$\mathcal{K} = g_x g_{yy} - 2 g_x g_y g_{xy} + g_y g_{xx}. \tag{19}$$

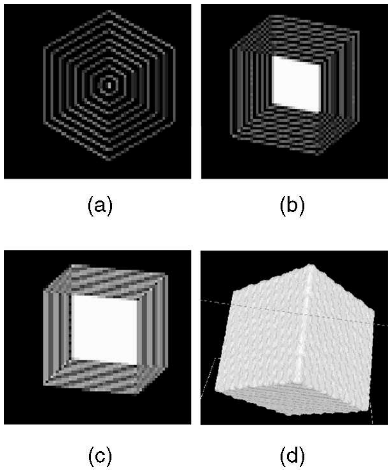

Fig. 11. Three-dimensional shape reconstruction for a synthetic cube: (a), (b), and (c) ETCs. (d) Reconstructed shape.

The cost function is minimized with the gradient search scheme. There are two major differences with the ART method. First, we do not convert the 2D image into a 1D array vector. Second, we only calculate the derivative of ϵ with respect to points in $b(A)$ and $b(\bar{A})$. These points are updated according to the following criteria:

1. If $\frac{\partial\epsilon}{\partial g(p)} > 0$ and $\frac{\partial\epsilon}{\partial g(\bar{p})} > 0$, change $g(p)$ from 1 to 0.
2. If $\frac{\partial\epsilon}{\partial g(\bar{p})} < 0$ and $\frac{\partial\epsilon}{\partial g(\bar{p})} < 0$, change $g(\bar{p})$ from 0 to 1.

The results of shape recovery for a synthetic and real object (of Fig. 2) are shown in Figs. 11 and 12, respectively.

5 CONCLUSION

In this paper, we introduced an imaging mode, in terms of equal thickness contours, that is being investigated for scientific studies. Next, we introduced a novel approach for shape recovery from multiple views and applied our approach to interference images of a sub-micron crystal structure. Our approach consists of three primary steps: 1) image representation in terms of contours corresponding to creases, 2) object thickness representation from contour data, and 3) shape recovery from object thickness obtained from each view. We are currently evaluating the accuracy of our approach with respect to a model system, with the objective of determining the number of views required to achieve a certain accuracy. Furthermore, since each view can produce up to two possible object thicknesses (depending on how the inner region is filled in), we are exploring various ways to select among these hypotheses, either during image acquisition or shape recovery. In addition, we plan to apply our method to other interference patterns obtained from natural outdoor scenes.

APPENDIX

THREE-DIMENSIONAL ALGEBRAIC RECONSTRUCTION

The 3D extension of the algebraic reconstruction of Section 5 is accomplished by replacing $g(i,j)$ of Fig. 10 with a cube $g(i,j,l)$, and the 1D projection $p(\theta,k)$ by a 2D projection $p(\vec{\theta},k_1,k_2)$, where $\vec{\theta} = (\theta_1,\theta_2,\theta_3)$ and θ_1, θ_2, and θ_3 correspond to the angle between the projection direction with the x, y, and z axes. The projection can now be computed by:

$$p(\vec{\theta},k_1,k_2) = \sum_{l=0}^{L} \frac{g(s_{k_1},s_{k_2},l)}{cos(\theta_3)}, \tag{20}$$

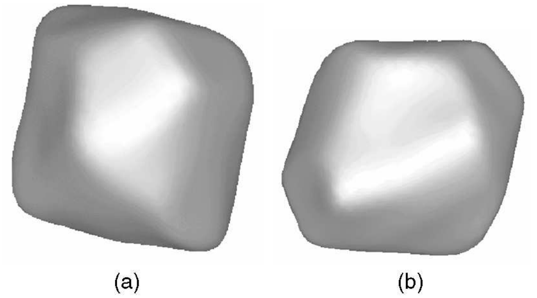

Fig. 12. Three-dimensional shape recovery from three views shown in Fig. 2: (a) View1. (b) View2.

where (s_{k_1},s_{k_2},l) is the point of intersection between the direction and plane $z=l$, $-\frac{\pi}{4} \le \theta_3 \le \frac{\pi}{4}$. $g(s_{k_1},s_{k_2},l)$ is a bilinear interpolation in the 2-by-2 neighborhood, and the projection is a linear combination of the image $g(i,j,l)$. The corresponding energy function is defined as:

$$\begin{aligned}\epsilon^2 = \sum_{n=0}^{N}\sum_{m_1=0}^{M_{1n}}\sum_{m_2=0}^{M_{2n}} (p(\vec{\theta}_n,m_1,m_2) - \mathcal{P}(\vec{\theta}_n,m_1,m_2))^2 \\ + \lambda \sum_{(i,j,l)\in b(A)} (\mathcal{K}(i,j,l))^2,\end{aligned} \tag{21}$$

where N is the number of projections of size M_{1n}-by-M_{2n} points and $\mathcal{K}$ is the product of mean curvature of the boundary surface and $|\bigtriangledown g|^3$. In 3D, we have

$$\begin{aligned}\mathcal{K} =& g_{xx}(g_y^2+g_z^2) + g_{yy}(g_x^2+g_z^2) + g_{zz}(g_x^2+g_y^2) \\ & - 2g_xg_yg_{xy} - 2g_xg_zg_{xz} - 2g_yg_zg_{yz}.\end{aligned} \tag{22}$$

ACKNOWLEDGMENTS

This work is supported by the Director, Office of Energy Science Research, Office of Computation and Technology Research, Mathematical, Information, and Computational Sciences Division, and Office of Basic Energy Sciences, Material Sciences Division of the US Department of Energy under contract no. DE-AC03-76SF00098 with the University of California. The LBNL publication number is 44263.

REFERENCES

[1] C. Allen, "Interferometric Synthetic Aperture Radar," *IEEE Geoscience and Remote Sensing Soc. Newsletter,* pp. 6-13, Sept. 1995.
[2] G. Aronsson, "On the Partial Differential Equation $u_x^2u_{xx} + 2u_xu_yu_{xy} + u_y^2u_{yy} = 0$," *Arikv för Matematik,* vol. 7, pp. 133-151, 1967.
[3] G. Aronsson, "On Certain Singular Solutions of the Partial Differential Equation $u_x^2u_{xx} + 2u_xu_yu_{xy} + u_y^2u_{yy} = 0$," *Manuscripta Math,* vol. 41, pp. 133-151, 1981.
[4] J. Boissonnat, "Shape Reconstruction from Planar Cross Sections," *Computer Vision, Graphics, and Image Processing,* vol. 44, no. 1, pp. 1-29, 1988.
[5] R.M. Bolle and B.C. Vemuri, "On Three-Dimensional Surface Reconstruction Methods," *IEEE Trans. Pattern Analysis and Machine Intelligence,* vol. 13, no. 1, pp. 1-13, Jan. 1991.
[6] G. Cong and B. Parvin, "Curve Evolution for Corner Enhancement," *Proc. Int'l Conf. Pattern Recognition,* 1998.
[7] G. Cong and B. Parvin, "Shape from Equal Thickness Contour," *Proc. Conf. Computer Vision and Pattern Recognition,* pp. 502-507, 1998.
[8] L. Evans, "Estimates for Smooth Absolutely Minimizing Lipschitz Extensions," *Electronic J. Differential Equations,* no. 3, pp. 1-9, 1993. http://ejde.math.swt.edu/Volumes/1993/03-Evans/abstr.html.
[9] G. Fornaro, G. Franceschetti, R. Lanari, and E. Sansosti, "Robust Phase-Unwrapping Techniques: A Comparison," *J. Optical Soc. Am., A,* vol. 13, pp. 2,355-2,366, 1996.
[10] G. Fornaro, G. Franceschetti, R. Lanari, E. Sansosti, and M. Tesanro, "Global and Local Phase-Unwrapping Techniques: A Comparsion," *J. Optical Soc. Am., A,* vol. 14, pp. 2,702-2,708, 1997.
[11] D. Gabor, "A New Microscopic Principle," *Nature,* 777, 1948.

[12] A. Gabriel, R. Goldstein, and H. Zebker, "Mapping Small Elevation Changes over Large Areas: Differential Radar Interferometry," *J. Geophysical Research,* vol. 94, no. B7, pp. 9,183-9,191, July 1989.
[13] R. Goldstein, H. Zebker, and C. Werner, "Satellite Radar Interferometry: Two-Dimensional Phase Unwrapping," *Radio Science,* vol. 23, no. 4, pp. 713-720, 1988.
[14] R. Gordon and G. Herman, "Reconstruction of Pictures from Their Projections," *Comm. ACM,* vol. 14, pp. 759-768, 1971.
[15] R. Kashyap and M. Mittal, "Picture Reconstruction for Projections," *IEEE Trans. Computers,* vol. 24, pp. 915-923, 1975.
[16] T. Kreis, "Digital Holographic Interference Phase Measurement Using the Fourier Transform Method," *J. Optical Soc. Am., A,* vol. 3, pp. 847-855, 1986.
[17] D. Massonnet, "The Displacement Field of the Landers Earthquake Mapped by Radar Interferometry," *Nature,* vol. 364, pp. 138-142, July 1993.
[18] D. Massonnet, "Satellite Radar Interferometry," *Scientific Am.,* vol. 276, no. 2, pp. 46-53, Feb. 1997.
[19] A. Mohammad-Djafari, K. Saner, Y. Khayi, and E. Cano, "Reconstruction of the Shape of a Compact Object from Few Projections," *Proc. Int'l Conf. Image Processing,* pp. 165-168, 1997.
[20] P. Saint-Marc, J. Chen, and G. Medioni, "Adaptive Smoothing: A General Tool for Early Vision," *IEEE Trans. Pattern Analysis and Machine Intelligence,* vol. 13, no. 6, pp. 514-530, June 1991.
[21] H. Takajo and T. Takahashi, "Least-Squares Phase Estimation from the Phase Difference," *J. Optical Soc. Am., A,* vol. 5, no. 3, pp. 416-425, 1988.
[22] A. Tonomura, *Progress in Holographic Interference Electron Microscopy.* North Holland, 1995.